JACS Au
AN OPEN ACCESS JOURNAL OF THE AMERICAN CHEMICAL SOCIETY

pubs.acs.org/jacsau
Article

Self-Organization of 1-Propanol at H-ZSM-5 Brønsted Acid Sites

Sungmin Kim,[‖] Mal-Soon Lee,*[,‖] Donald M. Camaioni, Oliver Y. Gutiérrez, Vassiliki-Alexandra Glezakou, Niranjan Govind, Thomas Huthwelker, Ruixue Zhao, Roger Rousseau, John L. Fulton,* and Johannes A. Lercher*

Cite This: *JACS Au* 2023, 3, 2487−2497

Read Online

ACCESS | Metrics & More | Article Recommendations | Supporting Information

ABSTRACT: In situ Al K-edge X-ray absorption near edge structure (XANES) and Extended X-ray absorption fine structure (EXAFS) spectroscopy in conjunction with ab initio molecular dynamics (AIMD) simulations show that adsorption of 1-propanol alters the structure of the Brønsted acid site through changes in the associated aluminum−oxygen tetrahedron in zeolite H-MFI. The decreasing intensity of the pre-edge signal of the in situ Al K-edge XANES spectra with increasing 1-propanol coverage shows that Al T-sites become more symmetric as the sorbed alcohol molecules form monomers, dimers, and trimers. The adsorption of monomeric 1-propanol on Brønsted acid sites reduces the distortion of the associated Al T-site, shortens the Al−O distance, and causes the formation of a Zundel-like structure. With dimeric and trimeric alcohol clusters, the zeolite proton is fully transferred to the alcohols and the aluminum−oxygen tetrahedron becomes fully symmetric. The subtle changes in Al−K-edge XANES in the presence of sorbate structures, with the use of theory, are used to probe the local zeolite structures and provide a basis to predict the population and chemical state of the sorbed species.

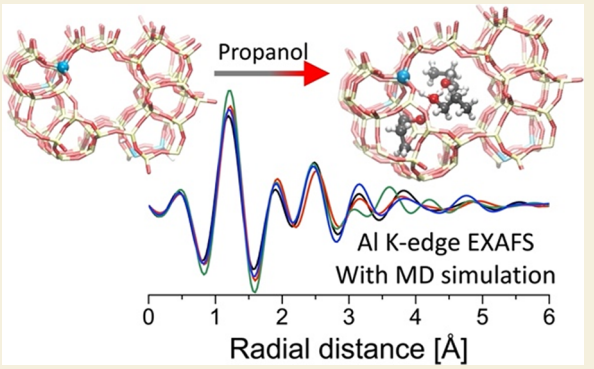

KEYWORDS: *in situ Al K-edge XAS, TD-DFT XANES, MD-EXAFS, AIMD simulation, adsorption on H-MFI, quantitative XANES analysis*

INTRODUCTION

Zeolites, crystalline microporous tectosilicates,[1−4] are widely used as sorbents and catalysts in which the Brønsted (BAS) and Lewis acid sites (LAS) reside within the crystalline pore network. The combination of high acid strength and the stabilization of initial and transition states by the nanopores lead to high activity for acid-catalyzed conversions.[5−16] The structural acid sites in zeolites are the consequence of the substitution of Si^{4+} by Al^{3+} cations at tetrahedral framework positions (Al T-sites), leading to negatively charged tetrahedra, with metal cations and a covalently bound H^+ balancing the negative charge.[17] The combination of the confinement, the specific bond angles of the Al−O bonds in the tetrahedron (and the subtle variations in the O−H bond strength as a consequence), and the stabilization of the adsorbed substrates influence the catalytic activity.[18−21]

Together, the Al T-site and the steric constraints of the zeolite micropore provide a unique environment. The adsorption of the substrate and solvent molecules at the Al T-site influences the local self-organization of both. For the case of water in the zeolite pore, at low water chemical potential, a single water molecule interacts with the Al T-site via hydrogen bonding. In the presence of a second water molecule, the proton is transferred to water forming a hydronium ion. Further water addition increases the hydration shell around the hydrated hydronium ion.[22−24] At their largest cluster size, hydrated hydronium ions containing approximately eight water molecules reside near the Al T-site of H-MFI.[25] The hydrated hydronium ions create a local ionic environment, which induces a strong nonideality and increases the excess chemical potential of adsorbed organic substrates compared to empty pores.[26,27] Hence, understanding the interactions and self-organization in the confined pores is crucial for designing new catalytic systems.

Alcohol dehydration is one of the primary steps in the conversion of biomass-derived compounds into liquid fuel and chemicals.[28−31] Mechanistic studies have proven that the interaction of the alcohol hydroxyl group with BAS initiates E1-like (stepwise) or E2-like (concerted) dehydration. Like water, alcohols bound to the BAS can either be fully protonated or share the proton of the BAS with the oxygen

Received: May 25, 2023
Revised: August 3, 2023
Accepted: August 18, 2023
Published: August 30, 2023

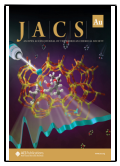

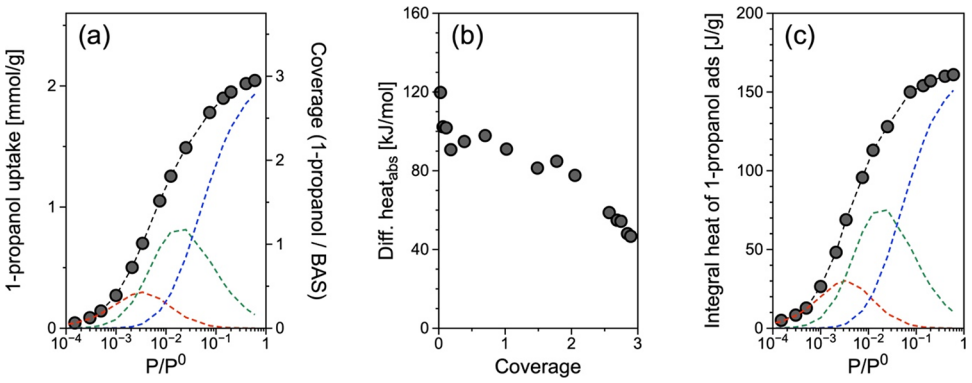

Figure 1. (a) 1-propanol uptake, (b) differential heat, (c) integral heat of adsorption of gas-phase 1-propanol on H-MFI at 50 °C, with monomer (---), dimer (---), and trimer (---) adsorption model. (P^0 = 0.02 bar).

of the zeolite framework. For example, methanol (on H-MFI) is only protonated in the presence of several methanol molecules forming protonated hydrogen-bonded methanol clusters.[28] Interestingly, a single ethanol molecule already shares a proton with the T-site oxygen. The addition of a second ethanol molecule completes the proton transfer (protonated dimer) that is hydrogen-bonded to the zeolite oxygens.[29] In an earlier study of 1-propanol, the formation of monomers and dimers was concluded from kinetic measurements, which showed a negative reaction order for dehydration and ether-forming reactions.[30] While the adsorption isotherm of 1-propanol on H-MFI quantifies three 1-propanol molecules per Brønsted acid site, how the third 1-propanol molecule organizes in the micropore along with 1-propanol monomer and dimer species remains elusive. Hence, resolving the configuration of the third 1-propanol is required to fully understand the molecular environment in the micropore, which is closely linked to catalytic reactivity.

In order to characterize this initial state of reacting alcohols, typically nuclear magnetic resonance (NMR) or infrared (IR) spectroscopy has been combined with ab initio molecular dynamics (AIMD) simulations, with the objective to resolve the structure of adsorbed alcohol molecules at the Al T-site.[29,31−33] However, these spectroscopic probes are not able to directly resolve the first-shell Al−O structure at the T-site nor the types of oligomeric alcohol species that reside in the pores at the vicinity of the T-site. X-ray absorption near-edge structure (XANES) and extended X-ray absorption fine structure (EXAFS) at the Al K-edge can be used to probe the average chemical state and local structure near the T-site.[34,35]

Al K-edge XANES probes the dipole transition of unoccupied states for a photoelectron excited from the Al 1*s* initial state. The Al K-edge XANES spectrum can be defined by three regions: the pre-edge (ΔE = −2 eV) assigned to Al 1s to Al 3d transitions, the rising edge assigned to the Al 1s to mixed Al 3p states (ΔE = 0 eV), and the "white line" (ΔE = +2 eV) having transitions from Al 1s to mixed Al 3p and O 3p states (or atoms of other pore ligands).[34] The intensity and position of pre-edge peak inform about the first-shell symmetry structure of Al in the T-site, i.e., $Al(O-Si-)_4^-$. Importantly, the white line results from a set of approximately 4−6 transitions to mixed ligand electronic states from the second and third coordination shells. This group of transitions represents a unique set of energy transitions and intensities that correspond to a precise set of atomic arrangements, including both within the framework and the nearby molecular species within the pores. The recent and remarkable implementation of time-dependent density functional theory (TDDFT) has enabled the interpretation of these long-range structural features to two or three solvation shells from the XANES spectrum. Thus, XANES has the possibility of probing the ordering of solutes and solvents in the zeolite pores in the vicinity of the Al T-site. In turn, computational spectroscopy combined with AIMD simulations is a powerful tool for translating the features of XAS spectra to the atomic scale structure.[35−37]

In this work, we evaluate the adsorption isotherm and adsorption heat of 1-propanol on H-MFI, which reveals 1-propanol trimer species formation along with 1-propanol monomer and dimer. AIMD simulations allow us to determine the Al T-site symmetry and adsorption configurations of alcohol species at experimental conditions. The structural data from the simulations enabled us to calculate ensemble averaged EXAFS (MD-EXAFS)[36] and XANES (MD-XANES) spectra using TDDFT. This powerful combination enabled us to construct models of active sites that contain information about static and dynamic disorder as well as anharmonic motions[38] and compare them directly with experimentally measured spectra to refine our understanding of the local environment at Al T-sites. As a result, we report the structures of adsorbed 1-propanol in H-MFI and how they change with varying the number of locally adsorbed molecules. Understanding the development of 1-propanol on H-MFI Al T-sites lays the basis for an atomistic-level understanding of acid-catalyzed dehydration rates.

RESULTS AND DISCUSSION

Quantitative Aspects of Adsorption of 1-Propanol

Adsorption isotherms and integral adsorption enthalpies of 1-propanol on H-MFI are compiled in Figure 1. The maximum 1-propanol uptake, close to 1-propanol vapor pressure, corresponds to the 2.05 $mmol_{1\text{-PrOH}}/g$ (Figure 1a), which is close to the value for the pore volume of micropores filled with liquid 1-propanol at normal density (2.13 $mmol_{1\text{-PrOH}}/g$). This saturation uptake corresponds to an average of three 1-propanol per Al T-site on the H-MFI used for this study (Si/Al = 15). The differential heat of adsorption as a function of 1-propanol coverage (Figure 1b) is displayed as a function of alcohol molecules per Al T-site (i.e., from 1 to 3). During the first exposure of H-MFI to gas phase 1-propanol (0−0.025 coverage), the heat of adsorption was −120 kJ/mol. This high

https://doi.org/10.1021/jacsau.3c00259
JACS Au 2023, 3, 2487−2497

Table 1. Comparing the Calculated Adsorption-Free Energies (ΔG°_{ads}), Enthalpies (ΔH°_{ads}) and Entropies (ΔS°_{ads}) of 1-Propanol Monomer, Dimer, and Trimer at 60 °C That Were Obtained From a QHA Using AIMD Simulations Compared to Those from the Experimental Values at 50 °C

	ΔG°_{ads} [kJ/mol]		ΔH°_{ads} [kJ/mol]		ΔS°_{ads} [J/mol/K]	
step	theory	experiment	theory	experiment	theory	experiment
$PrOH + H^+ \rightarrow PrOH_2^+$	−29	−27	−115	−101	−256	−230
$PrOH + PrOH_2^+ \rightarrow (PrOH)_2H^+$	−23	−24	−85	−83	−117	−181
$PrOH + (PrOH)_2H^+ \rightarrow (PrOH)_3H^+$	−14	−18	−65	−51	−75	−101

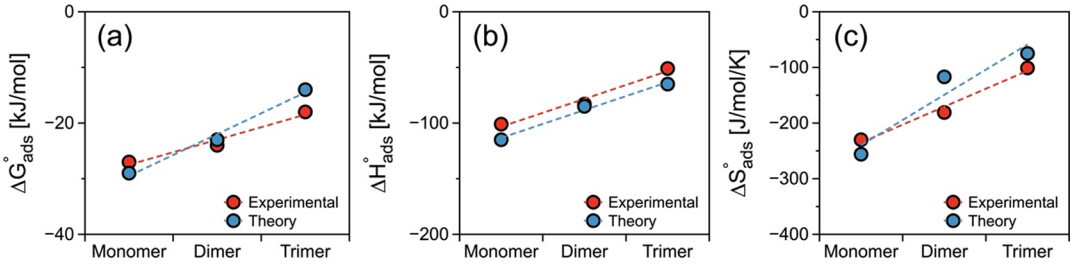

Figure 2. (a) Differential adsorption-free energies (ΔG°_{ads}) and deconvoluted (b) enthalpies (ΔH°_{ads}) and (c) entropies (ΔS°_{ads}) of 1-propanol monomer, dimer, and trimer at 60 °C obtained from a QHA using AIMD data (blue lines) compared with experimental values (red lines).

initial adsorption heat is attributed to the adsorption of 1-propanol on defect sites involving LAS.[39,40] The heat of adsorption was approximately at −115 kJ/mol for coverages from 0.065 to 1 and gradually decreased at higher coverages until reaching the enthalpy of condensation for 1-propanol (≈ −50 kJ/mol). Modeling the adsorption isotherms (Figure 1a) indicates that 1-propanol molecules continuously adsorb on Al T-site, forming monomers and dimers, while at high coverages 1-propanol molecules disperse in the zeolite pores. The high degree of pore filling makes it highly likely that the third alcohol molecule is associated via hydrogen bonding with two other molecules at the Al T-site at saturation uptake.

For the modeling adsorption isotherms, we hypothesize two adsorption models (Table S1), which differ in the site of adsorption of the third 1-propanol molecule, i.e., (i) trimer formation on Al T-site (Figure 1a) and (ii) independent adsorption of the third 1-propanol onto the framework (Figure S1e).

The trimer formation model (Figure 1a) assumes that 1-propanol molecules adsorb sequentially on the Al T-sites, forming monomers, dimers, and trimers. As the equilibrium distribution of adsorbed species shifts from monomers to trimers via dimers, the coverage and adsorption enthalpy of 1-propanol are subdivided as functions of 1-propanol partial pressure using the model shown in Table S1. It assumes a stepwise increase of adsorbates from monomers to trimers through three interlinked equilibria. We used this model to determine the equilibrium pressure that forms distinct surface species (Figure 1a), i.e., monomers ($\approx 2.0 \times 10^{-4}$ P/P^0), dimers ($\approx 1.0 \times 10^{-3}$ P/P^0), and trimers ($\approx 1.4 \times 10^{-1}$ P/P^0) on Al T-sites at 50 °C. The adsorption constants and coverages of 1-propanol species were determined from the adsorption isotherm (Figure 1a), which corresponds to the adsorption free-energies (ΔG°_{323K}) of −27, −24, and −18 kJ/mol for monomers, dimers, and trimers, respectively (Table 1 and Table S2). The adsorption enthalpies (ΔH°_{323K}) were calculated for monomer (−101 kJ/mol), dimer (−83 kJ/mol), and trimer (−51 kJ/mol) species by simultaneously fitting the integral adsorption isotherms for propanol uptake and the heat released (Figure 1a,c).

For the second model involving the independent 1-propanol adsorption on the framework (Table S3), the adsorption free energy and adsorption enthalpy of monomer (−27 and −102 kJ/mol, respectively) and dimer (−24 and −83 kJ/mol, respectively) are similar to the values obtained with the trimer model (Table S2). The model with 1-propanol monomer and dimer adsorption on BAS along with propanol molecular adsorption on the SiO_2 framework, however, has a higher adsorption enthalpy of −48 kJ/mol for adsorption of the third propanol molecule, although its adsorption free energy of −19 kJ/mol is not significantly different from trimer formation at Brønsted acidic Al T-sites. We estimated the entropic contributions (ΔS°_{323K}) from the adsorption free-energies and adsorption enthalpies: −230, −181, −101, and −90 J/mol/K for monomer, dimer, trimer, and 1-propanol on the framework species, respectively. This trend suggests that the monomer is strongly bound at an Al T-site, while the degrees of freedom of adsorbed 1-propanol are limited by the bulkiness of the adsorbed species in the steric constraints of the pore. As a comparison, the adsorption of 1-propanol on silicalite-1 per molecule is −14 and −66 kJ/mol of ΔG°_{323K} and ΔH°_{323K}, respectively, associated with the entropy loss of −162 J/mol/K (Figure S1). There is a constant adsorption enthalpy of 1-propanol on silicalite-1, regardless of the 1-propanol equilibrium pressure. Furthermore, the AIMD-calculated enthalpy of 1-propanol on silicalite-1 (−66 kJ/mol) is in line with the experiment; see structure in Figure S2. Hence, the adsorption enthalpy of 1-propanol on silicalite-1 is not due to 1-propanol local clustering around defect sites but is rather due solely to interactions between the alcohol and the zeolite framework.

The adsorption enthalpy of −48 kJ/mol for the third 1-propanol adsorbed onto H-MFI framework, i.e., the second model, is different from that of 1-propanol on the silicalite-1 (−66 kJ/mol). This finding demonstrates that this second model cannot explain experimental results. Unlike the nearly constant value on silicalite-1, the adsorption enthalpy, ΔH°_{323K}, decreased with H-MFI from −101 kJ/mol for the first 1-propanol adsorption to −51 kJ/mol for the third. This difference is attributed to the increasingly weaker interactions

https://doi.org/10.1021/jacsau.3c00259
JACS Au 2023, 3, 2487−2497

of additional alcohol molecules in dimers and trimers. The higher entropy losses observed on H-MFI per molecule of alcohol added reflect the self-organization of 1-propanol at the BAS. However, it is challenging to determine the configuration of the third 1-propanol molecule within the micropore by solely relying on the adsorption isotherm model.

Modeling the Adsorption of 1-Propanol on BAS

Standard free energy of 1-propanol adsorbed on H-MFI at 60 °C was determined using a quasi-harmonic approximation (QHA),[29,41,42] for which the vibrational density of states (VDOS) of bare and 1-propanol adsorbed H-MFI were calculated from the Fourier transform of the velocity autocorrelation function using AIMD data. The obtained VDOS and its discussion are compiled in Figure S3 and supplementary note S1, respectively. The calculated adsorption-free energies (ΔG°_{ads}) with deconvoluted enthalpy (ΔH°_{ads}) and entropy (ΔS°_{ads}) are shown in Table 1 and Figure 2. The adsorption-free energy (ΔG°_{ads}) decreases to −23 kJ/mol when 1-propanol is added to monomers, forming a dimer on Al T-sites, which was also seen in ethanol adsorption on H-MFI.[29] When one more 1-propanol is added to the dimer forming a trimer, the adsorption-free energy is −14 kJ/mol. The formation of the trimer also leads to a smaller change of entropy (−75 J/mol/K) compared to the formation of dimer (−117 J/mol/K).

Comparison between experimental and calculated values (Figure S4) reveals that the calculated ΔH°_{ads} values are overestimated compared to the experiments. The ΔS°_{ads} of monomers is underestimated, while the ΔS°_{ads} of the dimer and trimer are overestimated compared to the experimental values. The differences between theory and experiment are the smallest for the dimer for both ΔH°_{ads} (−3 kJ/mol) and ΔG°_{ads} (−1 kJ/mol), while the difference of ΔS°_{ads} is the smallest for monomer (−25 J/mol/K). These differences can be partly attributed to the coexistence of 1-propanol species observed in the experimental isotherm (Figure 1), while theory calculates the specific 1-propanol species.

Structural Analysis by AIMD Simulations

To study the adsorbed state of 1-propanol on BAS, a simulated annealing process on the final structure of AIMD trajectories was used. It allows obtaining the lowest energy structures (Figure 3 and the *xyz* coordinates reported in supplementary note S3). The 1-propanol monomer structure has the proton shared between the O of the Al T-sites (O_B) and the O of the 1-propanol (O_{Pr}), which is known as a Zundel-like configuration. When another 1-propanol is added, a linear dimer is formed, wherein the proton is fully transferred to the first 1-propanol forming a protonated propanol (Eigen-like structure) that interacts with O_B through a hydrogen bond. AIMD simulation also shows that the 1-propanol dimer, which resides at the junction between straight and sinusoidal channels, forms a protonated alcohol structure, i.e., Eigen-like structure, with a hydrogen bond to O_B at Al T-site (see Figure S5). The average energy of this configuration is comparable with that in the straight channel, see Figure 3, ($\Delta E \sim 15 \pm 5$ kJ/mol). From the thermodynamic point of view, this indicates the dimer can be adsorbed on Al T-site in both channels. A detailed discussion of all possible locations is, however, beyond the scope of this contribution. When the third 1-propanol molecule is added, a hydrogen-bonded open trimer forms, where two 1-propanol molecules occupy the straight channel and the other occupies a sinusoidal channel. The trimer is located near a T-site where the protonated 1-propanol interacts with other 1-propanol molecules via hydrogen bonds. It is worth noting that during the AIMD simulation, the trimer was formed via pore diffusion of a free 1-propanol (from an initial position away from the dimer), which then formed a hydrogen bond with the linear dimer. This process is shown as a movie in the SI. This sequence illustrates the preferable formation of the trimer in H-MFI at a higher partial pressure of 1-propanol.

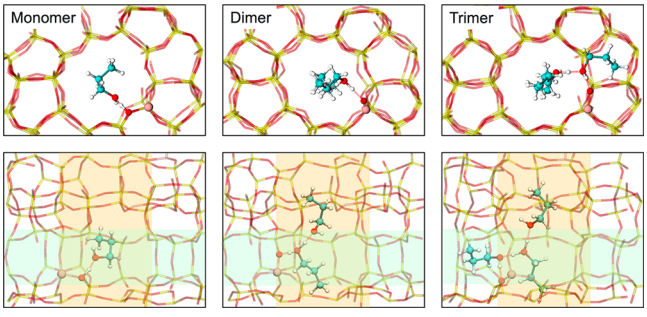

Figure 3. Lowest energy structures of 1-propanol adsorbed H-MFI were obtained from a slow annealing process using the last structure of AIMD simulations. The color code is Si-yellow, Al-pink, O-read, C-cyan, and H-white. The orange/green rectangle in the lower panel represents the straight and sinusoidal channels, respectively.

Various radial distribution functions (RDF), $g(R)$, from the AIMD trajectories, were calculated to understand the structural changes of 1-propanol adsorbed on H-MFI (Figures 4 and S6). As shown in Figure 4, the calculations provided average distances between different sets of species that implicitly include the dynamic properties of structures at 60 °C. For bare H-MFI, two distinct peaks at 1.72 and 1.96 Å were observed in $g(R)$ of Al−O_B (Figure 4a) due to the asymmetric Al−O tetrahedral structure caused by elongation of the single Al−O bond that hosts the proton. This 1.96 Å peak for the protonated T-site is also associated with the strong peak at 0.99 Å in $g(R)$ of O_B−H (Figure 4b).[34]

When a single 1-propanol was adsorbed on H-MFI, the Al−O_B distance becomes about 1.74 Å where a weak shoulder peak at ∼1.87 Å indicates contraction of Al−O_B distance observed for bare H-MFI (Figure 4a). For the bonded monomer, we also observed broad peaks at 1.1 and 1.3 Å in the $g(R)$ of O_B−H (Figure 4b) and O_{Pr}−H (Figure 4c), respectively, corresponding to proton sharing between O_B and O_{Pr} (the Zundel-like structure). Upon the formation of the 1-propanol dimer or trimer, the proton completely transfers to 1-propanol, forming a propoxonium ion hydrogen bonded to the zeolite oxygen (the Eigen-like structure), see Figure 3. Transfer of the proton leads to a nearly symmetric tetrahedral structure of AlO_4 as demonstrated by a sharp unimodal peak at 1.75 Å in the $g(R)$ for Al−O_B (Figure 4a). A similar sequence for the protonation of the dimer has been reported for ethanol and water on H-MFI.[29,43]

Increasing the number of interacting 1-propanol molecules increased the O_B−H distance, although both dimer and trimer still show correlated distances to the oxygens via hydrogen bonds at 1.6−2.0 Å (Figure 4b). The $g(R)$ of Al−O_{Pr} (Figure 4d) shows the same trends, indicating that 1-propanol moves away from the Al T-sites with an increasing number of 1-propanol molecules. Moreover, the $g(R)$ of Al−O_{Pr} (Figure 4d) shows two distinct peaks at 3.68 and 5.5 Å for the dimer,

https://doi.org/10.1021/jacsau.3c00259
JACS Au 2023, 3, 2487−2497

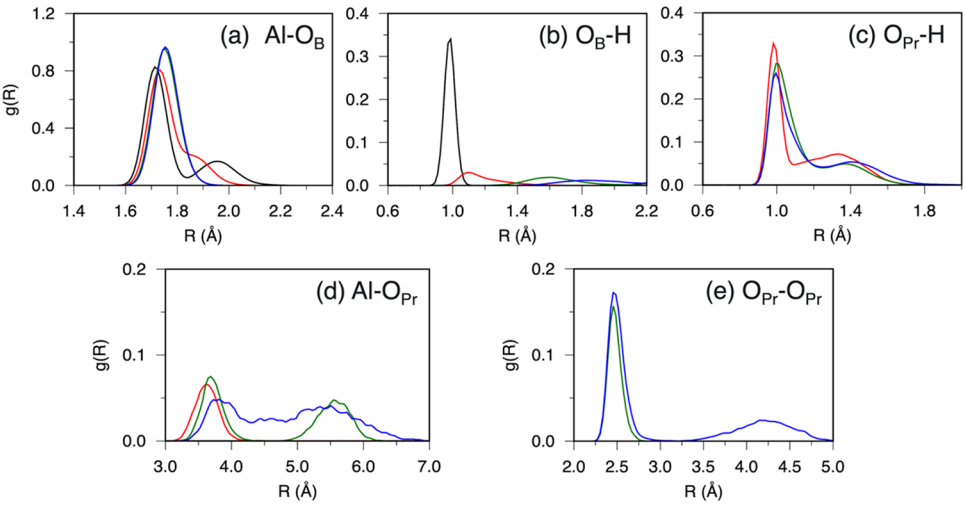

Figure 4. Calculated radial distribution functions, $g(R)$, showing the average distance between two species. B and Pr subscripts denote Al T-sites and 1-propanol, respectively. Color codes: black line − HMFI, red line − monomer, green line − dimer, blue line − trimer.

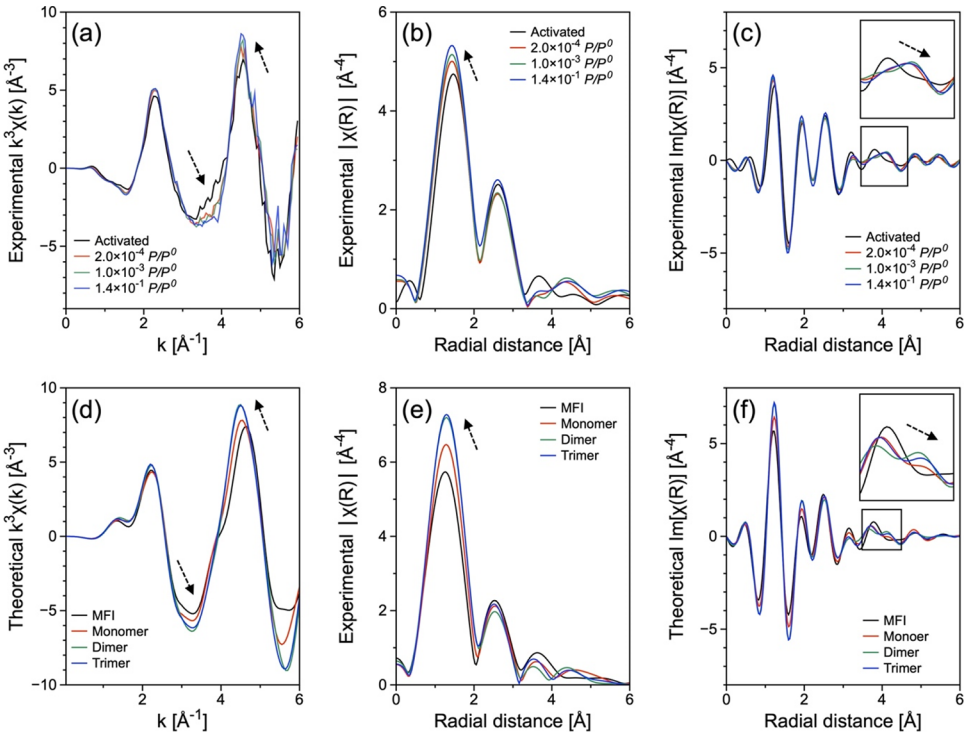

Figure 5. Al K-edge EXAFS: k^3-weighted (a, d) EXAFS, the magnitude (b, e) and imaginary (c, f) components of Fourier transform spectra from the experiment (a−c) and theory (d−f) for activated and 1-propanol adsorbed H-MFI. The insets in the imaginary Fourier transform show an elongation of the Al bond due to the Al−Si scattering of the H-MFI framework. The experimental Al K-edge EXAFS spectra were recorded at 2.0×10^{-4}, 1.0×10^{-3}, and 1.4×10^{-1} P/P^0 1-propanol pressure, corresponding to monomer, dimer, and trimer dominant regimes, respectively, in the adsorption isotherm. The arrows represent spectral changes with 1-propanol monomer, dimer, and trimer on Al T-site.

while the trimer shows three overlapped broad peaks at 3.76, 4.58, and 5.41 Å. This difference is caused by the distribution of 1-propanol near the T-site, i.e., a hydrogen-bonded open form of trimer compared to a linear form of the dimer as shown in Figure 3. Furthermore, the formation of trimer on H-MFI is strongly supported by $g(R)$ of O_{Pr}−O_{Pr}, showing the same distance of 2.45 Å for both dimer and trimer in addition to a peak at ∼4.2 Å for trimer (Figure 4e).

These observations demonstrate a significant rearrangement of 1-propanol as the number of alcohols at the binding site increases. The addition of 1-propanol to the Al T-site in the zeolite micropore causes the proton at the BAS to move away from the Al site forming a symmetric tetrahedron. When only a single alcohol is added, it shares the proton equally with the BAS. Protonated dimer formation results in proton transfers between the alcohols and, to a lesser extent, the BAS. However, protonated trimer formation leads to the opening up of the alcohol cluster, but proton transfers occur solely between the alcohol cluster. This is a dynamic process on the time scale of picoseconds, but the alcohol does not leave the vicinity of the Al during the entirety of the simulation time (>180 ps). This demonstrates that despite the increased fluctuation of the

https://doi.org/10.1021/jacsau.3c00259
JACS Au 2023, 3, 2487−2497

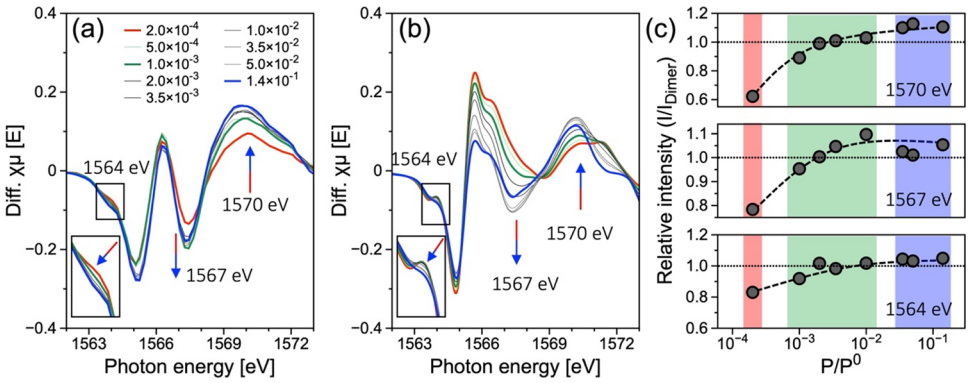

Figure 6. XANES difference spectra: (a) Experimental and (b) simulated Al K-edge XANES difference spectra of 1-propanol (2.0×10^{-4}–1.4×10^{-1} P/P^0) adsorbed H-MFI subtracted by activated H-MFI. The arrows indicate the observed changes with increasing 1-propanol pressure. The XANES spectra are generated using the weighted monomer–dimer–trimer distributions given in Figure 1. (c) Relative XANES intensity compared to that at 1.0×10^{-3} P/P^0 for 1564, 1567, and 1570 eV. The shade regions correspond to the dominant 1-propanol species of monomer, dimer, and trimer from Figure 1. In (b), distribution-corrected MD-XANES spectra are estimated using the linear combination of MD-XANES spectra for the monomer, dimer, and trimer based on the distributions shown in Figure 1 and Table S5, see details from the Computational Method section.

alcohol moieties, the entire cluster remains cohesive and anchored around the BAS.

Comparison of Experimental and MD Al K-Edge EXAFS Spectra

Figures 5a–c and S7 show the experimental EXAFS spectra at 60 °C for activated H-MFI and for H-MFI with increasing concentration of 1-propanol at pressures from 2.0×10^{-4} to 1.4×10^{-1} P/P^0. The activated H-MFI spectrum for the k^3-weighted EXAFS shows significant differences in the regions of k = 3.8 and 4.6 Å^{-1} that are associated with one long Al–O bond of the protonated T-site (Figures 5a and S7). Likewise, in the magnitude (Figure 5b) and the imaginary (Figure 5c) components of the Fourier transform for activated H-MFI spectrum, the average Al–O distance, corresponding to the features nominally at 1.5 Å is slightly elongated. The distance is decreased slightly due to the interaction of the proton on the Al T-site with 1-propanol species through either proton sharing with the monomer or protonation of the dimer or trimer. In the inset of Figure 5c, the 1-propanol-containing samples show an apparent elongation of the feature at 4 Å that is mostly attributed to the second shell Al–Si bond distance in the H-MFI framework.[35]

Likewise, in the imaginary component of the Fourier transform for activated H-MFI spectrum (Figure 5b), the average Al–O distance, corresponding to the features nominally at 1.5 Å, decreases very slightly in the presence of 1-propanol by the interaction of the proton on Al T-site with 1-propanol species through either proton sharing with the monomer or protonation of the dimer or trimer. In the inset of Figure 5b, the 1-propanol-containing samples show an apparent elongation of the feature at 4 Å that is mostly attributed to the Al–Si bond distance in the H-MFI framework.

The k^3-weighted EXAFS and Fourier-transformed EXAFS spectra derived from the AIMD trajectories are shown in Figure 5d–f. The MD-EXAFS calculation of H-MFI with 1-propanol adsorbed reproduces the relevant features and trends observed in experimental EXAFS spectra at 2.3, 3.8, and 4.5 Å^{-1} (Figure 5d) and the position and amplitude of the peaks in the magnitude (Figure 5e) and the imaginary (Figure 5f) components over the range from 1 to 6 Å. This indicates that the ensemble average configurations, corresponding to 60 °C that were used to generate the MD-EXAFS spectra, accurately reproduce the structural features in the experiment.

The MD-EXAFS spectra capture not only the structural response of the H-MFI framework but also scattering occurring as the concentration of 1-propanol in the pore is increased. As a final measure, we used the conventional method of fitting experimental spectra using theoretical standards in order to determine the average Al–O bond. As shown in Table S4 and Figure S8, the measured Al–O distance of 1.77 Å for the activated H-MFI agrees well with the value of 1.78 Å derived from $g(R)$. Further, the experimental Al–O distance of 1.74 and 1.73 Å for the monomer and dimer species, respectively, also agrees with the values of 1.74 and 1.75 from $g(R)$. The average Al–O distance contracts by about 0.04 Å (experiment and $g(R)$) as the proton of the Al T-site is increasingly shared with the 1-propanol thereby shortening one of the Al–O bonds. The experimental results help to confirm the structural transformation of the BAS as illustrated by $g(R)$.

It should be noted that the AIMD trajectory was calculated for one (T12) of 12 different T-sites that are located at different crystallographic positions, whereas the experiment samples incorporate the distribution of Al amongst all different T-sites. The major features of the EXAFS spectra in Figure 5 are due to the arrangement of the first four oxygens at the tetrahedral Al T-sites and changes in these Al–O bonds are largely due to different degrees of delocalization of the proton from the T-site. There is a very good agreement between the experimental EXAFS and the MD-EXAFS spectra, implying that the AlO_4 tetrahedra at the different T-sites mostly respond in a similar way to increasing concentrations of 1-propanol. In Figures 5b,d, the region from approximately 3.5–4.5 Å is primarily not only due to Al–Si bond distance of the framework but also contains a minor contribution from the scattering of 1-propanol in the pores. Here, the agreement between experiment and theory is not as good because the Al–Si structure in this longer-range region is known to be more dependent upon a particular T-site location.[35] Finally, while EXAFS is strongly dependent upon first-shell Al–O structure, the XANES response will have much greater sensitivity to longer-range 1-propanol structure in the pore. For this reason, the expectation is that the XANES response will be much more dependent on the choice of a particular T-site.

https://doi.org/10.1021/jacsau.3c00259
JACS Au 2023, 3, 2487–2497

Al K-Edge XANES and MD-XANES Analysis of 1-Propanol Adsorption

The Al K-edge XANES was used to determine changes in the local pore structure near the region of the Al T-site upon adsorption of 1-propanol (XANES spectra shown in Figures S9−S11 and discussions in S2). In particular, through the use of XANES difference spectra (Figure 6), it is possible to better evaluate only those changes that are associated with the ordering of 1-propanol within the pore. In other words, the significant contributions to the XANES spectra from the H-MFI framework have been mostly removed. The series of XANES difference spectra (Figure 6) with increasing 1-propanol adsorption (2.0×10^{-4} to 1.4×10^{-1} P/P^0) clearly show that there are changes induced by 1-propanol adsorption on the Al T-sites. Notably, for both experimental XANES (Figure 6a) and MD-XANES (Figure 6b), significant changes are observed at the pre-edge (1564 eV), the edge (1565 eV), and in the region of the white (1567−1570 eV).

With increasing 1-propanol pressure, the intensities of the pre-edge feature at 1564 eV and edge at 1565 eV are reduced which is indicated with arrows in Figure 6a,b. The pre-edge feature at 1564 eV is a highly local transition (Al 1s → 3d) that is sensitive to the immediate symmetry at the Al T-site. The intensity of this band increases significantly with distortion of the tetrahedral Al T-site symmetry. Hence, the observed intensity reduction in the pre-edge and edge regions for both experiment and theory is consistent with increasing symmetry of the tetrahedral T-site upon adsorption of the 1-propanol monomer, dimer, and trimer with increasing 1-propanol partial pressure. Further, these changes at 1564 eV coincide with the Al−O bond length changes that are detected with EXAFS (see Figure 5a,c) and RDF calculation (see Figure 4a).

In the region of the white line from 1567 to 1572 eV, the agreement between theory and experiment is less satisfactory. While the directions of the changes with increasing 1-propanol concentration are the same, the magnitude of the changes for the MD-XANES are much larger. The ability of TD-DFT to quantitatively predict the Al K-edge XANES intensities in these regions has been previously demonstrated for a zeolite[38] and for a series of Al standards.[44] In the MD-XANES spectra shown in Figure 6b, there are very significant and continuous changes in the band structure from about 1566 to 1572 eV in the transition from the monomer to the dimer and then the trimer. Based upon prior work,[34] this signal can be used to fingerprint the different hydrogen bonding structures within the pore adjacent to the T-site. The observed changes in this region for the experimental spectra are rather modest. Furthermore, the spectral deviation from 1-propanol dimer on the Al T-site sheds light on the configuration with the third 1-propanol molecule. The change of XAS spectra for Al T-site with dimer can be negligible when the third 1-propanol is adsorbed on the framework. However, the increase of 1-propanol pressure results in changes of the Al T-site (Figure 6c), which is a good agreement with the simulated Al K-edge XANES with trimer formation (Figure 6b). Therefore, we attribute this difference to the fact that the arrangement of monomers, dimers, and trimers will have different geometries in the different pore channels associated with each individual T-site in the H-MFI lattice. This hypothesis is supported by MD-XANES calculations for four different T-sites that show large differences in this region from 1570 to 1573 eV (see Figure S12a). Hence, for the experiment, the averaged XANES spectra for all T-sites are more muted than that for an individual T-site.

CONCLUSIONS

Combining in situ Al K-edge XAS spectroscopy and AIMD simulations with simulated MD-EXAFS and MD-XANES spectra provides a novel approach to define the structure of both adsorbed alcohols and the Al T-sites in zeolites. We show that subtle changes in EXAFS spectra can be understood by MD-EXAFS along with RDFs to describe the structure of Al T-sites interacting with oxygen and carbon from adsorbed 1-propanol species. The monomer 1-propanol forms a Zundel-like structure by sharing the proton with bridging oxygen in Al T-site. For the dimer and trimer, the proton is transferred to the alcohol cluster to form an Eigen-like structure. The proton transfer is also reflected in the increased symmetry of the Al T-site as the proton moves to the 1-propanol cluster, which is depicted as decreased intensity at pre-edge at 1564 eV of in situ and simulated Al K-edge XANES. In addition, in situ Al K-edge XANES in the white line region (1567−1572 eV) resolve the self-organization of 1-propanol species at the Al T-sites on H-MFI, which leads to a higher entropy loss by 1-propanol adsorption on H-MFI in comparison with that on silicate-1. The combination of in situ Al K-edge XANES, MD-EXAFS, and MD-XANES provide unequivocal evidence for the transition from monomers via dimers to trimers as the 1-propanol pressure increases, manifested by the increase in symmetry of the Al T-site. The insight into the ordering and the interactions allows us to provide a direct experimental and theoretical account of the structuring of reactive substrates in zeolite pores.

METHODS

Experimental Methods

H-MFI and AHFS Treatment. A commercial zeolite H-MFI (CBV3024E, Si/Al = 15) was treated with $(NH_4)_2SiF$ (AHFS) in order to minimize the concentration of extra-framework Al (EFAl) on the acidity and local environment of acid sites as following the procedure reported elsewhere.[30] The resulting material was then calcined at 550 °C for 5 h in synthetic air (100 mL/min and 10 °C/min).

Adsorption Isotherm. The adsorption of 1-propanol from the gas phase onto H-MFI was carried out using a Seteram TG-DSC 111 connected to a vacuum system and a pressure-controlled liquid vaporizing system. In a typical experiment, H-MFI (≈30 mg) was loaded on the microbalance and activated at 450 °C with 10 °C/min under vacuum (<10^{-4} mbar) for 1 h. After cooling down to 50 °C, 1-propanol vapor was stepwise injected through a dosing valve under an accurate control of the pressure into the system until equilibration. The weight increase and heat flux were monitored during pressure equilibration, where the 1-propanol pressure is normalized to 20 mbar of the vapor pressure (P^0) at 50 °C, which allows us to determine either gas or condensed phases. The heats of adsorption were directly obtained by integration of the recorded heat flux signal observed during the stepwise increase of 1-propanol pressure. The 1-propanol uptake and adsorption heat were then exploited for calculating the surface concentration and adsorption heat of 1-propanol species, i.e., monomer, dimer, and trimer. The adsorption model for monomer (m), dimer (d), and trimer (t) is tabulated in Table S1, where $[H^+]$ is the concentration of accessible Brønsted acid sites, i.e., Al-T site; $[C_3H_7OH]$ represents the 1-propanol pressure in gas phase; and coverage (θ).

In Situ Al K-Edge XAS Measurement. The Al K-edge X-ray absorption spectroscopy (XAS) experiments were performed at the PHOENIX II (Photons for the Exploration of Nature by Imaging and

https://doi.org/10.1021/jacsau.3c00259
JACS Au 2023, 3, 2487−2497

XAFS), elliptical undulator beamline at the Swiss Light Source (SLS) at the Paul Scherrer Institute (PSI), Switzerland. The energy calibration was achieved by setting the inflection point of an Al foil spectrum to 1559.6 eV. The pelletized, as-received H-MFI was mounted on a heated sample stage in the beamline vacuum chamber. For this study, the use of windows between the sample and the X-ray fluorescence detector was not required. To activate H-MFI, the cell was subsequently heated to 350 °C for 40 min and 400 °C for 20 min, respectively, with 5 °C/min of ramping rate. After cooling down to 60 °C, XAS spectra were acquired at Al K-edge (1405−1830 eV) using a double-crystal $KTiOPO_4$ (011) monochromator providing an energy resolution of about 0.6 eV over a scan range. Two Ni-coated mirrors were set at an angle of 1.45° to provide cutoff of higher harmonics. An unfocused 1.0 × 1.0 mm beam having a flux of ∼10^9 photons/s was used. The measurements were typically performed in fluorescence mode, where the X-ray fluorescence was detected using a 4-element Vortex Si-drift diode detector. The 1-propanol vapor from 0.02 to 2.8 mbar was introduced stepwise into the chamber through a dosing valve that allowed a precise, small aliquot of liquid to be injected into the ∼2 m^3 vacuum chamber that was accurately monitored with electronic vacuum pressure gage. The sample was pretreated by evacuation (6 × 10^{-3} mbar) and then activation at 400 °C. After cooling down to 60 °C, the XAS spectra were collected over a range of increasing 1-propanol pressure from 0.004 to 0.02 mbar. The resulting XAS spectra were processed and interpreted using Athena and Artemis software.[45] XANES normalization follows the standard protocol used within the Athena software. The pre-edge baseline is a linear line extending between −100 and −10 eV before the main edge, while the post-edge baseline was chosen between +25 and +150 eV above the edge. For the difference spectra, it is important that the starting point (+25) is at higher energy than the XANES evaluation region in order to avoid distorting the XANES spectra. Difference spectra were then obtained by subtracting the XANES spectrum of activated H-MFI from those recorded upon 1-propanol adsorption. For processing EXAFS spectra, a Fourier filter cutoff distance, R_{bkg}, of 1.0 Å was used during the background processing to extract the $\chi(k)$ data from the background function. The EXAFS data were then weighted by k^3 and truncated using a Hanning window with dk = 1.0 $Å^{-1}$ in the range of 1.5 < k < 6.0 $Å^{-1}$. We estimated the value of the core hole factor, S_0^2 = 1.0, from fits to the two crystalline standards of α-Al_2O_3 and $Na_2Al_2O_4$ standards. The S_0^2 factor typically had an error of ∼15%. For experimental EXAFS fitting, the theoretical scattering paths were obtained from the FEFF9 program.

Computational Methods

Computational Models. We started our simulations with H-MFI structure models used from a previous study,[30] which included the bare H-MFI and 1-propanol monomer and dimer adsorbed adjacent to the BAS with Al at T12 site. We also simulated a system of 1-propanol trimer on H-MFI which is generated by adding one more propanol to the propanol dimer system. The final structures used in this paper are the results of extensive AIMD simulations (>100 ps) followed by a simulated annealing process. All stationary structures obtained are reported in the SI.

DFT Calculations. Periodic density functional theory (DFT) calculations are performed within the generalized gradient approximation with the exchange-correlation functional of Perdew, Burke, and Ernzerhoff[46] as implemented in the CP2K package.[47,48] To take into account dispersion forces or van der Waals interactions, Grimme's third-generation corrections (DFT-D3) are used to describe energies more precisely.[49] Goedecker−Teter−Hutter pseudopotentials are used for the core electrons,[50] while the valence wave functions are expanded in terms of double-ζ quality basis sets optimized for condensed systems to minimize linear dependencies and superposition errors.[51] Electrostatic terms are calculated using an additional auxiliary plane-wave basis set with a 400 Ry cutoff. The Γ-point approximation is employed for the Brillouin zone integration because of the significant size of the supercell.

AIMD Simulations. DFT-based AIMD simulations were performed within the canonical NVT ensemble at 60 °C using a 0.5 fs time step and a Nosé−Hoover thermostat chain with a frequency of 4000 cm^{-1} to control the temperature to determine the local structure and their dynamic properties. For each system, we discard an initial 30−50 ps of trajectories to ensure the equilibration of the system. Then, well-equilibrated trajectories of 100 ps for bare H-MFI, >150 ps for hydrated H-MFI and 1-propanol (monomer, dimer, and trimer) on H-MFI were collected to obtain reliable statistical properties. Using the last configuration of simulation, we conducted a slow temperature annealing to obtain the lowest energy structure of each system, which can be found in Supplementary Information. The velocities obtained from AIMD trajectories were used to calculate the VDOS, using the Fourier transform of the velocity autocorrelation function:

$$D(\omega) = \int_0^\infty e^{-i\omega t}\langle V(\tau)\cdot V(\tau + t)\rangle dt$$

where v is the velocity, and the angular brackets indicate the statistical average over time. We then adopted a QHA approach[29,41,42] using calculated VDOS to estimate adsorption-free energetics for 1-propanol on H-MFI. The Gibbs free energies (ΔG_{ads}) and their enthalpic (ΔH_{ads}) and entropic (ΔS_{ads}) contributions of 1-propopanol adsorption are obtained using:

$$\Delta G_{ads} = \Delta H_{ads} - T\Delta S_{ads}$$

with

$$\Delta H_{ads} = \Delta E_{T=0K} + \Delta U_{trans} + \Delta U_{rot} + \Delta U_{vib} - RT$$

$$\Delta S_{ads} = \Delta S_{trans} + \Delta S_{rot} + \Delta S_{vib}$$

To better estimate ΔH_{ads}, $\Delta E_{T=0K}$ is calculated using TZV2PX basis sets for all atomic species except Al (TZV2P) and ΔH_{ads} is corrected for the PV term by subtracting the RT term.[29]

For ΔS_{ads}, S_{vib} is calculated using:

$$S_{vib} = 3k_B \int_0^\infty D(\omega)\left\{\frac{\hbar\omega}{2k_BT}\cot h\left(\frac{\hbar\omega}{2k_BT}\right) - \log\left[2\sin h\left(\frac{\hbar\omega}{2k_BT}\right)\right]\right\} d\omega$$

where $D(\omega)$ is calculated VDOS. Our previous work[29] has shown that the QHA can provide very good estimates of free energetics for ethanol adsorption on H-ZSM-5, where a detailed method can be found.

MD-EXAFS Simulations. We simulated K-edge MD-EXAFS spectra with FEFF8.5 program[52] using ≥1500 snapshots extracted from NVT trajectories with an equally spaced time interval of 0.05 ps for each system. For each system, each snapshot was used to calculate a full set of scattering (single and multiple scattering) paths for all atoms within 6.5 Å of each Al site. We then calculated the ensemble average of these scattering paths, which were directly compared with the experimental spectra. This approach has led to a quantitative treatment of all photoelectron single and multiple scattering paths, generating an EXAFS spectrum that captures all the structural details inherent in the MD simulation, including the bond lengths, bond angles, vibrational disorder, and local symmetry about the Al site(s). Since dynamic fluctuations are an intrinsic part of the sampling, the simulations implicitly include an exact treatment of the Debye-Waller factors in the EXAFS simulations.

MD-XANES Calculations with Time-Dependent DFT. Excited state XANES calculations were performed at the Al K-edge using a TDDFT-based restricted excitation window approach[53,54] as implemented in the NWChem quantum chemistry program.[54,55] This approach involves defining a model subspace of single excitations from the relevant core orbitals and is a valid ansatz because core excitation energies are well separated from pure valence−valence excitations. For each Al site conformation, the Sapporo-QZP-2012 all-electron basis set was used for the Al atom and the surrounding O atoms.[56,57] Si, C, and the other O atoms were represented with the

https://doi.org/10.1021/jacsau.3c00259
JACS Au 2023, 3, 2487−2497

Stuttgart RLC ECPs, while H atoms were represented with the STO-3G.[58] Although we have used a primary basis set for H atoms, the effect of the basis set for H atoms is negligible on XANES spectra, as shown in S3 and Figure S12 in SI. The exchange correlation was treated with the BHLYP functional[59] for consistency with our previous publication.[34,59] All boundary O atoms with unsatisfied bonds were passivated with H atoms. These methods have been used in our previous studies where the location and nature of the XANES spectral features were precisely predicted.[34,35] We generated finite-size clusters consisting of 108 atoms for H-MFI as the zeolite framework and adsorbed 1-propanol in addition using ≥100 snapshots extracted from AIMD trajectories that were equally spaced by 1.0 ps at 60 °C, the experimental condition. Similar size of the clusters has been used to represent the zeolite framework environment.[34,35,60] All calculated spectra were Lorentzian broadened by 0.8 eV and shifted by +16.5 eV to match the experimental pre-edge peak. To directly compare experimental XANES spectra which depend on 1-propanol pressure, we estimated distribution-corrected MD-XANES spectra where MD-XANES spectra for the monomer, dimer, and trimer are weighted by their distributions (d) (see Table S5) using $\chi_\mu(p) = \sum_i d_i \times \chi_i$ where $\chi_\mu(p)$ is distribution-corrected MD-XANES spectra at pressure p, d_i is the number of each 1-propanol species i (i = H-MFI, monomer, dimer, and trimer) at the given pressure p, and χ_i is calculated MD-XANES for each 1-propanol species.

The variations in the detailed structure of the T-sites significantly alter the XANES response.[35] In this study, T-site 12 was chosen in the simulations since it is reported to dominate Al substitution sites.[61,62] The generally broader features of the experimental XANES spectra with respect to the MD-XANES are the contributions from the collective ensemble of Al in different T-sites. MD-XANES and MD-EXAFS spectra of bare H-MFI with different T-sites show insignificant differences in their peak positions (Figure S13). This has also been reported for HBEA.[35] It is noteworthy that static calculations of XANES and EXAFS using the lowest energy structure cannot capture features shown in both experimental and MD XANES and EXAFS spectra as shown in S4 and Figures S14 and S15 in SI, demonstrating the importance of MD-XAS calculations to compare with experimental XAS which cannot achieve with static calculations.

■ ASSOCIATED CONTENT

Supporting Information

The Supporting Information is available free of charge at https://pubs.acs.org/doi/10.1021/jacsau.3c00259.

Equilibrium adsorption isotherm expressions for 1-propanol adsorption on H-MFI; thermochemistry for adsorption of 1-propanol on HZSM-5 30-AHFSa at 50 °C ; EXAFS fitting results ; distribution of 1-propanol species for distribution-corrected MD-XANES spectra calculation; adsorption isotherm and differential heats of 1-propanol adsorption on HMFI and silicalite-1 ; snapshot of 1-propanol adsorbed silicalite-1; simulated vibrational spectra from AIMD at 60 °C and difference spectra; comparison between experimental and calculated enthalpy and entropy; snapshot of a dimer at respective straight and sinusoidal channels; calculated radial distribution functions, $g(R)$; k^3-weighted $\chi(k)$ and the back-transformed k^3-weighted $\chi(q)$ of experimental EXAFS; fitting of k^3-weighted EXAFS; in situ and ensemble-averaged Al K-edge XANES; ensemble averaged Al XANES spectra and (b) pre-edge region corresponding to activated and 1-propanol adsorbed H-MFI at 60 °C; selective (a) in situ and (b) simulated Al K-edge XANES difference spectra; AlK-edge XANES with different basis sets; ensemble averaged Al K-edge XANES and EXAFS at different T-sites of bare HMFI; Al K-edge XANES and EXAFS of the lowest energy structure; calculated vibrational density of states; adsorption nature of 1-propanol on Al T-site; coordinates of the lowest energy structures (PDF)

■ AUTHOR INFORMATION

Corresponding Authors

Mal-Soon Lee − *Institute for Integrated Catalysis and Physical Science Division, Pacific Northwest National Laboratory, Richland, Washington 99354, United States;* orcid.org/0000-0001-6851-177X; Email: MalSoon.Lee@pnnl.gov

John L. Fulton − *Institute for Integrated Catalysis and Physical Science Division, Pacific Northwest National Laboratory, Richland, Washington 99354, United States;* orcid.org/0000-0001-9361-9803; Email: Fulton@pnnl.gov

Johannes A. Lercher − *Institute for Integrated Catalysis and Physical Science Division, Pacific Northwest National Laboratory, Richland, Washington 99354, United States; Department of Chemistry and Catalysis Research Institute, TU München, 85748 Garching, Germany;* Email: Johannes.Lercher@pnnl.gov

Authors

Sungmin Kim − *Institute for Integrated Catalysis and Physical Science Division, Pacific Northwest National Laboratory, Richland, Washington 99354, United States;* orcid.org/0000-0001-6602-1320

Donald M. Camaioni − *Institute for Integrated Catalysis and Physical Science Division, Pacific Northwest National Laboratory, Richland, Washington 99354, United States;* orcid.org/0000-0002-2213-0960

Oliver Y. Gutiérrez − *Institute for Integrated Catalysis and Physical Science Division, Pacific Northwest National Laboratory, Richland, Washington 99354, United States;* orcid.org/0000-0001-9163-4786

Vassiliki-Alexandra Glezakou − *Institute for Integrated Catalysis and Physical Science Division, Pacific Northwest National Laboratory, Richland, Washington 99354, United States;* Present Address: Chemical Science Division, Oak Ridge National Laboratory, Oak Ridge, Tennessee 37830, United States (V.-A.G., R.R.); orcid.org/0000-0001-6028-7021

Niranjan Govind − *Institute for Integrated Catalysis and Physical Science Division, Pacific Northwest National Laboratory, Richland, Washington 99354, United States;* orcid.org/0000-0003-3625-366X

Thomas Huthwelker − *Swiss Light Source, Paul Scherrer Institut (PSI), 5232 Villigen, Switzerland*

Ruixue Zhao − *Department of Chemistry and Catalysis Research Institute, TU München, 85748 Garching, Germany*

Roger Rousseau − *Institute for Integrated Catalysis and Physical Science Division, Pacific Northwest National Laboratory, Richland, Washington 99354, United States;* Present Address: Chemical Science Division, Oak Ridge National Laboratory, Oak Ridge, Tennessee 37830, United States (V.-A.G., R.R.); orcid.org/0000-0003-1947-0478

Complete contact information is available at: https://pubs.acs.org/10.1021/jacsau.3c00259

Author Contributions

[‖]S.K. and M.-S.L. contributed equally to this work.

https://doi.org/10.1021/jacsau.3c00259
JACS Au 2023, 3, 2487−2497

Notes

The authors declare no competing financial interest.

■ ACKNOWLEDGMENTS

This work was supported by the U.S. Department of Energy (DOE), Office of Science, Office of Basic Energy Sciences, Division of Chemical Sciences, and Geosciences & Biosciences (FWP 47319). PNNL is a multiprogram national laboratory operated for DOE by Battelle under Contract DE-AC05-76RL01830. Computational Resources were provided by user proposals at the Molecular Sciences Computing Facility (MSCF) in the William R. Wiley Environmental Molecular Sciences Laboratory, a US Department of Energy (DOE) national scientific user facility sponsored by the DOE's Office of Biological and Environmental Research and located at PNNL, and the National Energy Research Scientific Computing Center (NERSC), a U.S. Department of Energy Office of Science User Facility located at Lawrence Berkley National Laboratory (LBNL).

■ REFERENCES

(1) Barthomeuf, D. A general hypothesis on zeolites physicochemical properties. Applications to adsorption, acidity, catalysis, and electrochemistry. *J. Phys. Chem.* **1979**, *83*, 249−256.
(2) Jacobs, P. A.; Leuven, K. U. Acid zeolites: An attempt to develop unifying concepts. *Catal. Rev.* **1982**, *24*, 415−440.
(3) Feast, S.; Lercher, J. A. Synthesis of intermediates and fine chemicals using molecular sieve catalysts. In *Stud. Surf. Sci. Catal.*, Chon, H.; Woo, S. I.; Park, S. E., Eds.; Elsevier, 1996; Vol. *102*, pp 363−412.
(4) Lercher, J. A.; Jentys, A.; Brait, A. Catalytic test reactions for probing the acidity and basicity of zeolites. In *Acidity and Basicity*; Springer, 2008; pp 153−212.
(5) Ilias, S.; Bhan, A. Mechanism of the catalytic conversion of methanol to hydrocarbons. *ACS Catal.* **2013**, *3*, 18−31.
(6) Choi, M.; Na, K.; Kim, J.; Sakamoto, Y.; Terasaki, O.; Ryoo, R. Stable single-unit-cell nanosheets of zeolite MFI as active and long-lived catalysts. *Nature* **2009**, *461*, 246−249.
(7) Svelle, S.; Joensen, F.; Nerlov, J.; Olsbye, U.; Lillerud, K.-P.; Kolboe, S.; Bjørgen, M. Conversion of methanol into hydrocarbons over zeolite H-ZSM-5: Ethene formation is mechanistically separated from the formation of higher alkenes. *J. Am. Chem. Soc.* **2006**, *128*, 14770−14771.
(8) Alexopoulos, K.; John, M.; Van der Borght, K.; Galvita, V.; Reyniers, M.-F.; Marin, G. B. DFT-based microkinetic modeling of ethanol dehydration in H-ZSM-5. *J. Catal.* **2016**, *339*, 173−185.
(9) Calsavara, V.; Baesso, M. L.; Fernandes-Machado, N. R. C. Transformation of ethanol into hydrocarbons on ZSM-5 zeolites modified with iron in different ways. *Fuel* **2008**, *87*, 1628−1636.
(10) Takahashi, A.; Xia, W.; Nakamura, I.; Shimada, H.; Fujitani, T. Effects of added phosphorus on conversion of ethanol to propylene over ZSM-5 catalysts. *Appl. Catal., A* **2012**, *423*−*424*, 162−167.
(11) Mellmer, M. A.; Sanpitakseree, C.; Demir, B.; Bai, P.; Ma, K.; Neurock, M.; Dumesic, J. A. Solvent-enabled control of reactivity for liquid-phase reactions of biomass-derived compounds. *Nat. Catal.* **2018**, *1*, 199−207.
(12) Fraenkel, D.; Cherniavsky, M.; Ittah, B.; Levy, M. Shape-selective alkylation of naphthalene and methylnaphthalene with methanol over H-ZSM-5 zeolite catalysts. *J. Catal.* **1986**, *101*, 273−283.
(13) Ahn, J. H.; Kolvenbach, R.; Al-Khattaf, S. S.; Jentys, A.; Lercher, J. A. Methanol usage in toluene methylation with medium and large pore zeolites. *ACS Catal.* **2013**, *3*, 817−825.
(14) Dai, W.; Sun, X.; Tang, B.; Wu, G.; Li, L.; Guan, N.; Hunger, M. Verifying the mechanism of the ethene-to-propene conversion on zeolite H-SSZ-13. *J. Catal.* **2014**, *314*, 10−20.
(15) Allotta, P. M.; Stair, P. C. Time-resolved studies of ethylene and propylene reactions in zeolite H-MFI by in-situ fast IR heating and UV Raman spectroscopy. *ACS Catal.* **2012**, *2*, 2424−2432.
(16) Andrei, R. D.; Popa, M. I.; Fajula, F.; Cammarano, C.; Al Khudhair, A.; Bouchmella, K.; Mutin, P. H.; Hulea, V. Ethylene to propylene by one-pot catalytic cascade reactions. *ACS Catal.* **2015**, *5*, 2774−2777.
(17) Corma, A. Inorganic solid acids and their use in acid-catalyzed hydrocarbon reactions. *Chem. Rev.* **1995**, *95*, 559−614.
(18) Davis, M. E. New vistas in zeolite and molecular sieve catalysis. *Acc. Chem. Res.* **1993**, *26*, 111−115.
(19) Margarit, V. J.; Osman, M.; Al-Khattaf, S.; Martínez, C.; Boronat, M.; Corma, A. Control of the reaction mechanism of alkylaromatics transalkylation by means of molecular confinement effects associated to zeolite channel architecture. *ACS Catal.* **2019**, *9*, 5935−5946.
(20) Janda, A.; Vlaisavljevich, B.; Lin, L.-C.; Smit, B.; Bell, A. T. Effects of zeolite structural confinement on adsorption thermodynamics and reaction kinetics for monomolecular cracking and dehydrogenation of n-butane. *J. Am. Chem. Soc.* **2016**, *138*, 4739−4756.
(21) Dai, W.; Zhang, S.; Yu, Z.; Yan, T.; Wu, G.; Guan, N.; Li, L. Zeolite structural confinement effects enhance one-pot catalytic conversion of ethanol to butadiene. *ACS Catal.* **2017**, *7*, 3703−3706.
(22) Mei, D.; Lercher, J. A. Mechanistic insights into aqueous phase propanol dehydration in H-ZSM-5 zeolite. *AIChE J.* **2017**, *63*, 172−184.
(23) Joshi, K. L.; Psofogiannakis, G.; van Duin, A. C. T.; Raman, S. Reactive molecular simulations of protonation of water clusters and depletion of acidity in H-ZSM-5 zeolite. *Phys. Chem. Chem. Phys.* **2014**, *16*, 18433−18441.
(24) Bordiga, S.; Regli, L.; Lamberti, C.; Zecchina, A.; Bjørgen, M.; Lillerud, K. P. FTIR Adsorption Studies of H_2O and CH_3OH in the Isostructural H-SSZ-13 and H-SAPO-34: Formation of H-Bonded Adducts and Protonated Clusters. *J. Phys. Chem. B* **2005**, *109*, 7724−7732.
(25) Eckstein, S.; Hintermeier, P. H.; Zhao, R.; Baráth, E.; Shi, H.; Liu, Y.; Lercher, J. A. Influence of hydronium ions in zeolites on sorption. *Angew. Chem., Int. Ed.* **2019**, *58*, 3450−3455.
(26) Pfriem, N.; Hintermeier, P. H.; Eckstein, S.; Kim, S.; Liu, Q.; Shi, H.; Milakovic, L.; Liu, Y.; Haller, G. L.; Baráth, E.; Liu, Y.; Lercher, J. A. Role of the ionic environment in enhancing the activity of reacting molecules in zeolite pores. *Science* **2021**, *372*, 952.
(27) Milaković, L.; Hintermeier, P. H.; Liu, Y.; Baráth, E.; Lercher, J. A. Influence of intracrystalline ionic strength in MFI zeolites on aqueous phase dehydration of methylcyclohexanols. *Angew. Chem., Int. Ed.* **2021**, *60*, 24806−24810.
(28) Mirth, G.; Lercher, J. A.; Anderson, M. W.; Klinowski, J. Adsorption complexes of methanol on zeolite ZSM-5. *J. Chem. Soc., Faraday Trans.* **1990**, *86*, 3039−3044.
(29) Alexopoulos, K.; Lee, M.-S.; Liu, Y.; Zhi, Y.; Liu, Y.; Reyniers, M.-F.; Marin, G. B.; Glezakou, V.-A.; Rousseau, R.; Lercher, J. A. Anharmonicity and confinement in zeolites: Structure, spectroscopy, and adsorption free energy of ethanol in H-ZSM-5. *J. Phys. Chem. C* **2016**, *120*, 7172−7182.
(30) Zhi, Y.; Shi, H.; Mu, L.; Liu, Y.; Mei, D.; Camaioni, D. M.; Lercher, J. A. Dehydration pathways of 1-propanol on HZSM-5 in the presence and absence of water. *J. Am. Chem. Soc.* **2015**, *137*, 15781−15794.
(31) Solcà, N.; Dopfer, O. IR spectrum and structure of protonated ethanol dimer: Implications for the mobility of excess protons in solution. *J. Am. Chem. Soc.* **2004**, *126*, 9520−9521.
(32) Kondo, J. N.; Ito, K.; Yoda, E.; Wakabayashi, F.; Domen, K. An ethoxy intermediate in ethanol dehydration on Brønsted acid sites in zeolite. *J. Phys. Chem. B* **2005**, *109*, 10969−10972.
(33) Wang, W.; Jiao, J.; Jiang, Y.; Ray, S. S.; Hunger, M. Formation and decomposition of surface ethoxy species on acidic zeolite Y. *ChemPhysChem* **2005**, *6*, 1467−1469.

https://doi.org/10.1021/jacsau.3c00259
JACS Au 2023, 3, 2487−2497

(34) Vjunov, A.; Wang, M.; Govind, N.; Huthwelker, T.; Shi, H.; Mei, D.; Fulton, J. L.; Lercher, J. A. Tracking the chemical transformations at the Brønsted acid site upon water-induced deprotonation in a zeolite pore. *Chem. Mater.* **2017**, *29*, 9030−9042.
(35) Vjunov, A.; Fulton, J. L.; Huthwelker, T.; Pin, S.; Mei, D.; Schenter, G. K.; Govind, N.; Camaioni, D. M.; Hu, J. Z.; Lercher, J. A. Quantitatively probing the Al distribution in zeolites. *J. Am. Chem. Soc.* **2014**, *136*, 8296−8306.
(36) Palmer, B. J.; Pfund, D. M.; Fulton, J. L. Direct modeling of EXAFS spectra from molecular dynamics simulations. *J. Phys. Chem.* **1996**, *100*, 13393−13398.
(37) Lee, I.; Lee, M.-S.; Tao, L.; Ikuno, T.; Khare, R.; Jentys, A.; Huthwelker, T.; Borca, C. N.; Kalinko, A.; Gutiérrez, O. Y.; Govind, N.; Fulton, J. L.; Hu, J. Z.; Glezakou, V.-A.; Rousseau, R.; Sanchez-Sanchez, M.; Lercher, J. A. Activity of Cu−Al−Oxo extra-framework clusters for selective methane oxidation on Cu-exchanged zeolites. *JACS Au* **2021**, *1*, 1412−1421.
(38) Collinge, G.; Yuk, S. F.; Nguyen, M.-T.; Lee, M.-S.; Glezakou, V.-A.; Rousseau, R. Effect of collective dynamics and anharmonicity on entropy in heterogenous catalysis: Building the case for advanced molecular simulations. *ACS Catal.* **2020**, *10*, 9236−9260.
(39) Lee, C. C.; Gorte, R. J.; Farneth, W. E. Calorimetric study of alcohol and nitrile adsorption complexes in H-ZSM-5. *J. Phys. Chem. B* **1997**, *101*, 3811−3817.
(40) Thamm, H. Calorimetric study on the state of C_1−C_4 alcohols sorbed on silicalite. *J. Chem. Soc., Faraday Trans. 1* **1989**, *85*, 1−9.
(41) Yuk, S. F.; Lee, M.-S.; Collinge, G.; Zhang, J.; Padmaperuma, A. B.; Li, Z.; Polo-Garzon, F.; Wu, Z.; Glezakou, V.-A.; Rousseau, R. Mechanistic understanding of catalytic conversion of ethanol to 1-butene over 2D-Pillared MFI zeolite. *J. Phys. Chem. C* **2020**, *124*, 28437−28447.
(42) De Sousa, R. L.; Leite Alves, H. W. Ab initio calculation of the dynamical properties of PPP and PPV. *Braz. J. Phys.* **2005**, *36*, 501−504.
(43) Wang, M.; Jaegers, N. R.; Lee, M.-S.; Wan, C.; Hu, J. Z.; Shi, H.; Mei, D.; Burton, S. D.; Camaioni, D. M.; Gutiérrez, O. Y.; Glezakou, V.-A.; Rousseau, R.; Wang, Y.; Lercher, J. A. Genesis and stability of hydronium ions in zeolite channels. *J. Am. Chem. Soc.* **2019**, *141*, 3444−3455.
(44) Fulton, J. L.; Govind, N.; Huthwelker, T.; Bylaska, E. J.; Vjunov, A.; Pin, S.; Smurthwaite, T. D. Electronic and Chemical State of Aluminum from the Single-(K) and Double-Electron Excitation (KLII&III, KLI) X-ray Absorption Near-Edge Spectra of α-Alumina, Sodium Aluminate, Aqueous Al3+·(H2O)6, and Aqueous Al(OH)4. *J. Phys. Chem. B* **2015**, *119*, 8380−8388.
(45) Ravel, B.; Newville, M. ATHENA, ARTEMIS, HEPHAESTUS: data analysis for X-ray absorption spectroscopy using IFEFFIT. *J. Synchrotron Radiat.* **2005**, *12*, 537−541.
(46) Perdew, J. P.; Burke, K.; Ernzerhof, M. Generalized gradient approximation made simple. *Phys. Rev. Lett.* **1996**, *77*, 3865.
(47) Kühne, T. D.; Iannuzzi, M.; Del Ben, M.; Rybkin, V. V.; Seewald, P.; Stein, F.; Laino, T.; Khaliullin, R. Z.; Schütt, O.; Schiffmann, F.; Golze, D.; Wilhelm, J.; Chulkov, S.; Bani-Hashemian, M. H.; Weber, V.; Borštnik, U.; Taillefumier, M.; Jakobovits, A. S.; Lazzaro, A.; Pabst, H.; Müller, T.; Schade, R.; Guidon, M.; Andermatt, S.; Holmberg, N.; Schenter, G. K.; Hehn, A.; Bussy, A.; Belleflamme, F.; Tabacchi, G.; Glöß, A.; Lass, M.; Bethune, I.; Mundy, C. J.; Plessl, C.; Watkins, M.; VandeVondele, J.; Krack, M.; Hutter, J. CP2K: An electronic structure and molecular dynamics software package - Quickstep: Efficient and accurate electronic structure calculations. *J. Chem. Phys.* **2020**, *152*, 194103.
(48) VandeVondele, J.; Krack, M.; Mohamed, F.; Parrinello, M.; Chassaing, T.; Hutter, J. Quickstep: Fast and accurate density functional calculations using a mixed Gaussian and plane waves approach. *Comput. Phys. Commun.* **2005**, *167*, 103−128.
(49) Grimme, S.; Antony, J.; Ehrlich, S.; Krieg, H. A consistent and accurate ab initio parametrization of density functional dispersion correction (DFT-D) for the 94 elements H-Pu. *J. Che. Phys.* **2010**, *132*, 154104.
(50) Goedecker, S.; Teter, M.; Hutter, J. Separable dual-space Gaussian pseudopotentials. *Phys. Rev. B* **1996**, *54*, 1703.
(51) VandeVondele, J.; Hutter, J. Gaussian basis sets for accurate calculations on molecular systems in gas and condensed phases. *J. Chem. Phys.* **2007**, *127*, 114105.
(52) Ankudinov, A. L.; Ravel, B.; Rehr, J. J.; Conradson, S. D. Real-space multiple-scattering calculation and interpretation of x-ray-absorption near-edge structure. *Phys. Rev. B* **1998**, *58*, 7565−7576.
(53) Lopata, K.; Van Kuiken, B. E.; Khalil, M.; Govind, N. Linear-response and real-time time-dependent density functional theory studies of core-level near-edge X-ray absorption. *J. Chem. Theory Comput.* **2012**, *8*, 3284−3292.
(54) Valiev, M.; Bylaska, E. J.; Govind, N.; Kowalski, K.; Straatsma, T. P.; Van Dam, H. J. J.; Wang, D.; Nieplocha, J.; Apra, E.; Windus, T. L.; de Jong, W. A. NWChem: A comprehensive and scalable open-source solution for large scale molecular simulations. *Comput. Phys. Commun.* **2010**, *181*, 1477−1489.
(55) Henkelman, G.; Arnaldsson, A.; Jónsson, H. A fast and robust algorithm for Bader decomposition of charge density. *Comput. Mater. Sci.* **2006**, *36*, 354−360.
(56) Noro, T.; Sekiya, M.; Koga, T. Segmented contracted basis sets for atoms H through Xe: Sapporo-(DK)-nZP sets (n = D, T, Q). *Theor. Chem. Acc.* **2012**, *131*, 1124.
(57) Sekiya, M.; Noro, T.; Koga, T.; Shimazaki, T. Relativistic segmented contraction basis sets with core-valence correlation effects for atoms 57La through 71Lu: Sapporo-DK-nZP sets (n = D, T, Q). *Theor. Chem. Acc.* **2012**, *131*, 1247.
(58) Pritchard, B. P.; Altarawy, D.; Didier, B.; Gibson, T. D.; Windus, T. L. New Basis Set Exchange: An open, up-to-date resource for the molecular sciences community. *J. Chem. Inf. Model.* **2019**, *59*, 4814−4820.
(59) Becke, A. D. A new mixing of Hartree−Fock and local density-functional theories. *J. Chem. Phys.* **1993**, *98*, 1372−1377.
(60) Sklenak, S.; Dědeček, J.; Li, C.; Wichterlová, B.; Gábová, V.; Sierka, M.; Sauer, J. Aluminum siting in silicon-rich zeolite frameworks: A combined high-resolution 27Al NMR spectroscopy and quantum mechanics / molecular mechanics study of ZSM-5. *Angew. Chem., Int. Ed.* **2007**, *46*, 7286−7289.
(61) Olson, D. H.; Khosrovani, N.; Peters, A. W.; Toby, B. H. Crystal structure of dehydrated CsZSM-5 (5.8Al): Evidence for nonrandom aluminum distribution. *J. Phys. Chem. B* **2000**, *104*, 4844−4848.
(62) Kim, C. W.; Heo, N. H.; Seff, K. Framework sites preferred by aluminum in zeolite ZSM-5. Structure of a fully dehydrated, fully Cs^+-exchanged ZSM-5 crystal (MFI, Si/Al = 24). *J. Phys. Chem. C* **2011**, *115*, 24823−24838.

https://doi.org/10.1021/jacsau.3c00259
JACS Au 2023, 3, 2487−2497